lubricants

MDPI

Article

Time-Resolved Characterization of Dynamic Tribochemical Processes for Dicationic Imidazolium Ionic Liquid

Roman Nevshupa [1,*], Marcello Conte [2], Silvia Guerra [3] and Elisa Roman [3]

1 Spanish National Research Council, Institute "Eduardo Torroja" (IETCC-CSIC), C/Serrano Galvache 4, 28033 Madrid, Spain
2 Anton Paar TriTec SA, Rue de la Gare 4, 2034 Peseux, Switzerland; marcello.conte@anton-paar.com
3 Spanish National Research Council, Institute of Material Science of Madrid (ICMM-CSIC), C/Sor Juana Inés de la Cruz 3, 28049 Madrid, Spain; silvia.guerra@csic.es (S.G.); eroman@icmm.csic.es (E.R.)
* Correspondence: r.nevshupa@csic.es; Tel.: +34-913-020-440

Received: 16 June 2017; Accepted: 20 July 2017; Published: 25 July 2017

Abstract: Dynamic tribochemical processes for dicationic ionic liquid containing a geminal imidazolium cation head group bridged by a poly(ethylene glycol) and a bis(trifluoromethylsulfonyl)imide anion were studied using time-resolved mechanically stimulated gas emission mass-spectrometry (MSGE-MS). In comparison with similar monocationic imidazolium ionic liquids with short alkyl or long polyether side chains, the dicationic ionic liquid had a lower coefficient of friction on Ti6Al4V alloy and smoother behavior. The analysis of volatile decomposition products suggested multiple tribochemical reactions in which both anionic and cationic moieties are involved. The tribochemical degradation of cations was mainly through the detachment of the side and bridging chains from the imidazolium head groups. The absence of volatile products containing nitrogen implies that the imidazole group remained unchanged. Hydrogen and water desorption were attributed to the reactions of hydrogen fluoride being a product of anion degradation with titanium and titanium oxide, respectively.

Keywords: ionic liquids; dicationic; imidazolium; poly(ethylene glycol); tribochemistry; mechanically stimulated gas emission mass-spectrometry

1. Introduction

Room-temperature ionic liquids (ILs) are salt structures consisting of large cation and anion moieties, which are characterized by melting temperatures below 100 °C. In tribological applications, ILs have demonstrated superior performance as lubricants under both mixed and boundary conditions [1–9]. In severe environments, in space and at high temperatures, IL-base lubricants are especially propitious due to their exceptional thermal stability, both oxidative and nonoxidative [10–14]. During the last decade, imidazolium-base ionic liquids with fluorinated anions have been specially addressed in a number of studies [1,15–17]. The application range of the imidazolium ILs was further expanded by rational designing of the molecular structure and the side chains offering the possibility of obtaining versatile ILs with tailored polarity, hydrophobicity, and corrosive and antioxidant properties [7,18–25]. Generally, the increase of the length of the alkyl side chains attached to a cation head group leads to the improvement of wear resistance, but this effect is not straightforward [2,22,26]. Substitution of alkyl chains by poly(ethylene glycol) (PEG) improved the tribological performance of the IL, although at the cost of decreasing its thermal stability [8,27]. Another approach relies on bridging two cationic head groups by PEG chain. Molecular dynamics simulation and advanced spectroscopy have revealed significant differences in structural heterogeneity and nano-organization between monocationic and geminal dicationic ILs with a long connecting chain [28–31] that was

associated with better tribological properties, higher stability, lower toxicity and corrosiveness of the dicationic ILs [14,31–41].

In the literature, there is a consensus of opinions that the good friction-reduction and wear-resistant properties of ILs are owed to their ability to form stable adsorbed layers and protective tribo-films [4,27,42–44]. For ILs with fluorinated anions, Jimenez et al. [26] noted that the formation of a metal fluoride-rich boundary tribolayer is necessary to achieve good tribological performance. Cai et al. [8] studied the changes in the chemical composition of a steel surface subjected to rubbing under PEG lubrication with various imidazolium IL additives and provided the evidence for complicated tribochemical reactions leading to the formation of iron oxides, fluorides and sulphates. Physical adsorption of nitrogen double-bond compounds on a steel surface was also reported [45]. Mahrova et al. [46] showed that the tribofilms formed by some pyridimiun-based dicationic ILs with a PEG bridging chain were able to significantly reduce friction in comparison with glycerol base stock, but had a much higher wear rate. However, in most of the studies the steps of the tribochemical processes that lie behind remain poorly understood. In a large measure, this is due to the low yield and selectivity of tribochemical reactions [11] and the lack of a broadly available experimental technique for the time-resolved characterization of tribochemical reactions at a buried interface. In the vast majority of experimental studies, a *post mortem* approach has been employed that consists of analyzing possible chemical changes on the worn surfaces, wear debris, and in the lubricants, once a tribological test is accomplished [7,11,47].

A new family of experimental techniques that combine tribometry with mass spectrometry or surface sensitive techniques has recently emerged [48–54]. These new techniques can provide important information on the development of tribochemical processes in the course of a tribological test. In the present work, we probed tribochemical processes in dicationic imidazolium ionic liquid with a PEG_{500} bridging chain and bis(trifluoromethylsulfonyl)imide (NTf_2) anion on Ti6Al4V substrate using mechanically stimulated gas emission (MSGE) mass spectrometry. This material was selected for the substrate because of the technological implications [26] and to contrast the results of this study with previous works [26,44,46]. The tribochemical reactions were analyzed through measurement of the composition and emission kinetics of volatile products as a function of the normal load and test duration. The products of tribochemical reactions were identified using statistical and correlation analyses. The results were compared with the tribochemical behavior of an homologous monocationic ionic liquid [27,44].

2. Experimental

2.1. Materials

Dicationic geminal imidazolium IL with a poly(ethylene glycol) (PEG_{500}) bridging chain and a bis(trifluoromethanesulfonyl)imide anion was synthesized and kindly provided by Dr. M. Mahrova [46,55]. The structures of the dicationic IL (IL2-di) and its monocationic analogue (IL2), which was used as a benchmark in this study, are shown in Figure 1.

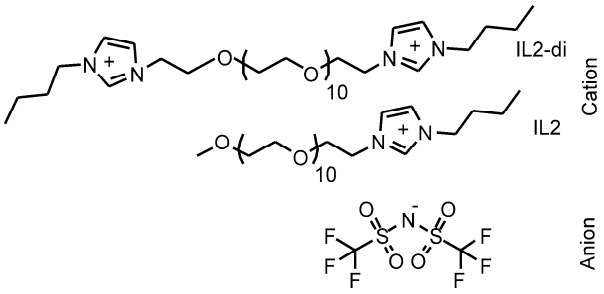

Figure 1. Molecular structures of the dicationic IL and analogue monocationic IL.

A 1 µL drop of IL was supported on a titanium flat sheet. The pin was an alumina ball, 3 mm in diameter. Before each experiment both the substrate and the pin were ultrasonically degreased in acetone and ethanol bath. To eliminate the adsorbed water and air-borne carbonaceous contamination, the pin was etched in a hot Piranha solution (three parts of concentrated sulphuric acid and one part of 30% hydrogen peroxide solution) for several minutes.

2.2. Experimental Techniques and Procedures

Tribological characterization and analysis of mechanically stimulated gas emission were carried out using an original ultrahigh vacuum system [49,50]. A friction cell with a reciprocating pin-on-flat configuration was specially designed to obtain almost zero intrinsic gas emission. For the sake of comparison with the reference IL, the friction force was measured under the same conditions as in the work [44]: the normal load was 9.8 N and the mean linear velocity was 2.7 mm/s. The composition of the emitted gases was analysed by a quadrupole mass spectrometer. During MSGE measurements, the force gauges were off to avoid cross talk, while the experimental conditions were changed to optimize the operating conditions for the mass spectrometer: to avoid amplifier overloading, to reduce contamination of the electron multiplier by volatile organic compounds, and to enhance the dynamic response. For MSGE measurements the normal load was 0.9–1.8 N and the mean sliding velocity was 0.18 m/s. A diaphragm of well-defined molecular conductance situated between a vacuum chamber and a pumping line and provided for the quantification of the rate of gas emission using a dynamic gas expansion method [56].

High stability of the residual gas pressure is crucial for the accurate measuring of tiny pressure variations associated with MSGE. Therefore, the system was pumped for 48–72 h until the variation of the mass-spectrometer signals was below 3%/h. With the residual pressure stabilized, the reference mass spectrum of residual gases was obtained. For this purpose, five or more mass spectra were measured. These data was organized in a matrix with N columns representing the spectral components with different mass-to-charge ratios, m/z, and n_r rows representing the samples of the mass spectra. The sample mean and the sample standard error were determined column-wise, yielding the vectors of size N of a reference mean mass spectrum, RMS, and a reference standard error, RSE, correspondingly.

Mechanically stimulated gas emission was studied by measuring the mass spectra in the course of rubbing and for several hundreds of seconds after its end. The return of all mass-spectrometry signals to their initial background level was chosen as a criterion for measurement ending. The matrix of the measured data, **MS**, had n rows corresponding to MSGE mass spectra of each N channel. Differential mass spectra, DMS, characterizing the emitted gases that were obtained by subtracting the reference spectrum RMS from each row of the matrix **MS**:

$$\|dms_{i,j} = ms_{i,j} - rms_j\|_{i=\overline{1,n};j=\overline{1,N};} \quad (1)$$

A t-test (H_0: $dms_{i,j} = 0$ and H_1: $dms_{i,j} \neq 0$) was used to check the statistical significance of the values of DMS [27]. A statistics $\frac{dms_{i,j}}{rse_i}$ was compared with the critical value of Student's distribution, $t_{k,\alpha}$, where $k = n_r$ is the number of degrees of freedom and α is the significance level. The null hypothesis was accepted if

$$\frac{dms_{i,j}}{rse_i} \leq t_{k,\alpha} \quad (2)$$

When a highly dynamic emission process is measured by a mass spectrometer, the sequential form of the channel's measuring may lead to a significant increase in the data variation. This may hamper the correct identification of the volatile components which give rise to the registered mass-spectra. To face this problem a behavioral analysis of the mass-spectroscopic signals was developed [44,57] and applied in this work. The method is based on the hypothesis that the signals showing the same behavior of the time series should originate from the same precursors. For this purpose the DMS was resized by removing null columns, i.e., the null components of the differential mass spectra, and then the

Pearson correlation coefficient, r, was calculated for each pair of the DMS components.The statistical significance of r was analyzed using the hypothesis test with H_0: $r = 0$ and H_1: $r \neq 0$. The null hypothesis was rejected if the corresponding p-value was below α.

3. Results and Discussion

The behavior of the friction coefficient of IL2-di is shown in Figure 2a. The friction coefficient rapidly stabilized without pronounced run-in. The steady coefficient of friction (COF) was about 0.2, slightly lower than for the homologous monocationic IL2 (see Figure 2b). For comparison, the COF for the homologous monocationic IL2 and IL1 (1-butyl-3-methylimidazolium bis(trifluoromethanesulfonyl)imide) adopted from the work [58] are also shown in Figure 2b. For IL2-di, the COF decreased by 30% with respect to the monocationic IL with alkyl side chains, and by 10% with respect to the monocationic IL with a methoxy PEG side chain. These results are in line with literature [14,36,46].

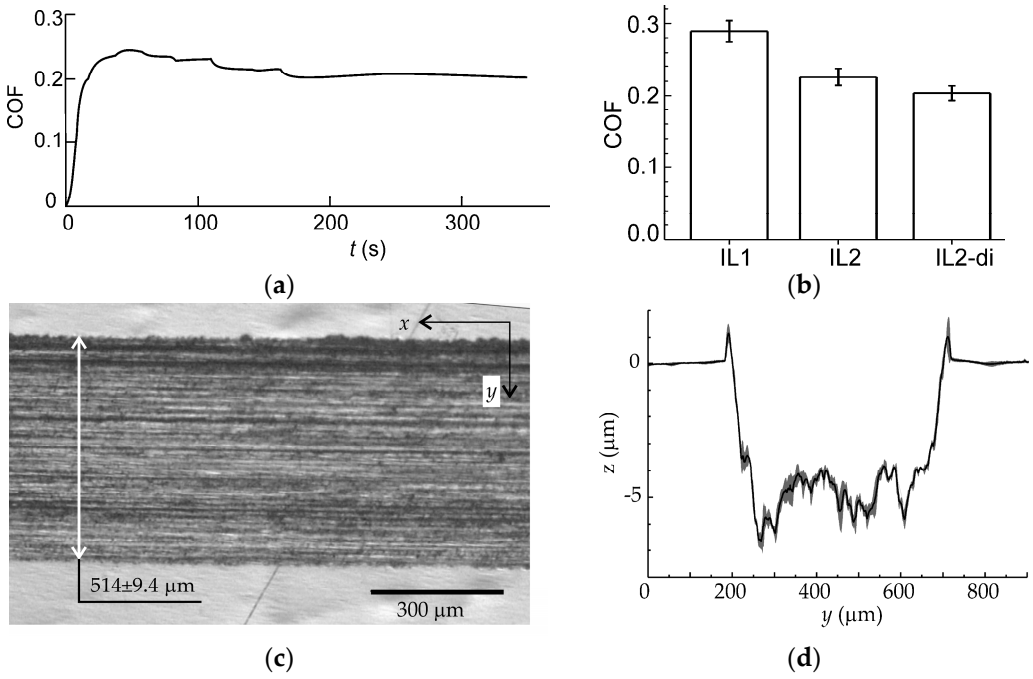

Figure 2. (**a**) Time series of friction coefficient for dicationic IL2-di; (**b**) Mean coefficient of friction (COF) and standard error of mean for IL2-di. The data for two homologous monocationic IL2 and IL1 (1-butyl-3-methylimidazolium bis(trifluoromethanesulfonyl)imide) from [44] are also shown for the comparison; (**c**) Optical image of the worn surface after the tribological test; (**d**) Mean cross-section profile of the wear track. The shaded area depicts the confidence interval ($\alpha = 0.05$).

The worn surface (Figure 2c) showed longitudinal abrasion marks. The mean cross-section profile is shown in Figure 2d by a solid line, while the shaded area depicts the confidence interval. The surface morphology was irregular across the wear track (large variation of height along y), but quite regular in the longitudinal direction (x), which follows from the relatively small spread of the confidence interval. Blakish pileups on the sides of the wear track should be related with the products of tribochemical reactions rather than with plastic deformation of the substrate. The presence of blakish deposits on the valleys between the longitudianl marks also points on the possible tribofilm formation. The wear of the tribofilm together with the substrate corrosion/tribocorrosion could be the reason for the change in the color and transparency of the IL2-di, which turned black and opaque after the test. Despite the absence of evident corrosion signs immediately after the friction test, corrosion pits appeared on the whole sample surfaces, both rubbed and not, when the samples were kept covered by IL2-di for several days after the test. The possible mechanisms of corrosion will be discussed at the end of this section.

The differential mass spectra of the volatile products emitted from IL2-di during rubbing (see Figure 3) presented similitude with the DMS of IL2, which were reported previously [44]. For both IL2 and IL2-di the spectral components can be classified into the four groups shown in Table 1.

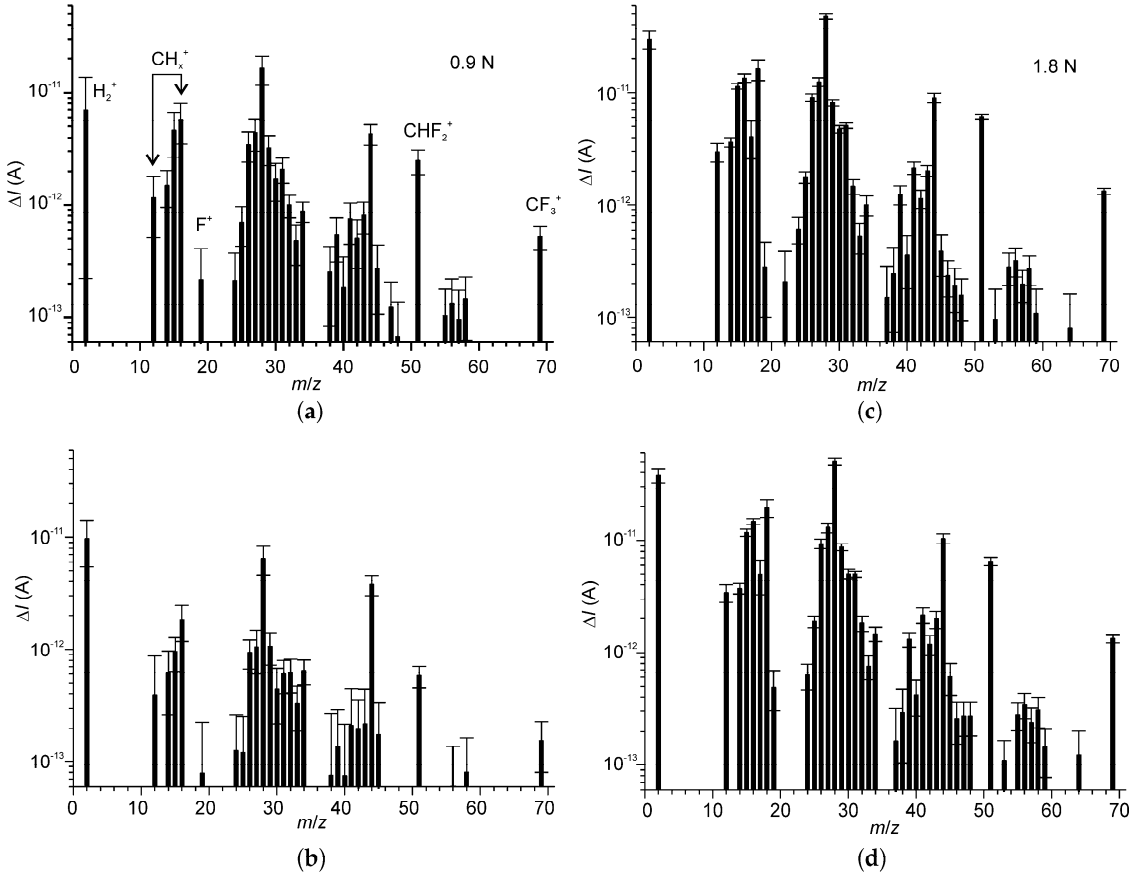

Figure 3. Mean differential mass-spectra (DMS) of emitted volatile products of the tribochemical reactions with IL2-di as function of the normal load: (**a**,**b**) 0.9 N; (**c**,**d**) 1.8 N. All DMS were obtained during rubbing: (**a**,**c**) correspond to the initial stage of the test; (**b**,**d**) correspond to the final stage of the test.

Table 1. Groups of the components of DMS of IL2-di.

Group	*m*/*z*	Possible Precursors
A	19, 31, 32, 51, 69	CF_3, CF_xH_y [1)], PEG fragments (31, 32)
B	12–16	CH_4, CH_3*, CH_3^+
C	24–34, 39–45, 55–58	PEG, alkanes
D	2, 17, 18	H_2, H_2O

[1)] The precursors can include molecules, molecular radicals and ions emitted from the surface.

The group of ions A can be ascribed to volatile compounds originating from the trifluoromethyl detachment from the anion, while the ions at m/z 31 and 32 could also have contributions from PEG fragments. The component at m/z 51 was the most intensive in this group. The signal m/z 50 was excluded from the DMS after the significance test since the null hypothesis was not rejected. This finding contrasts the results obtained for monocationic IL2, for which both m/z 50 and 51 were statistically significant [44]. It also suggests that after detachment from the anion, trifluoromethane recombines with H and reaches the mass spectrometer as fluoroform rather than carbon tetrafluoride or trifluoromethyl radical. This is supported by the observation that the relative intensities of the signals at m/z 50, 51 and 69 are in reasonable compliance with the corresponding components of

the fragmentation patterns for CHF_3 [59] (Figure 4). The large difference between the experimental data and the reference spectra for the signals at m/z 31, 32 can be ascribed to the contributions from CH_3O^+ and CH_4O^+, respectively. Notwithstanding this difference, the experimental data is closer to the fragmentation pattern of fluoroform, than CF_4. The signal of F^+ at m/z 19 was weak in all cases, and the differences between the experimental spectrum and the fragmentation patterns were within the measurement uncertainty.

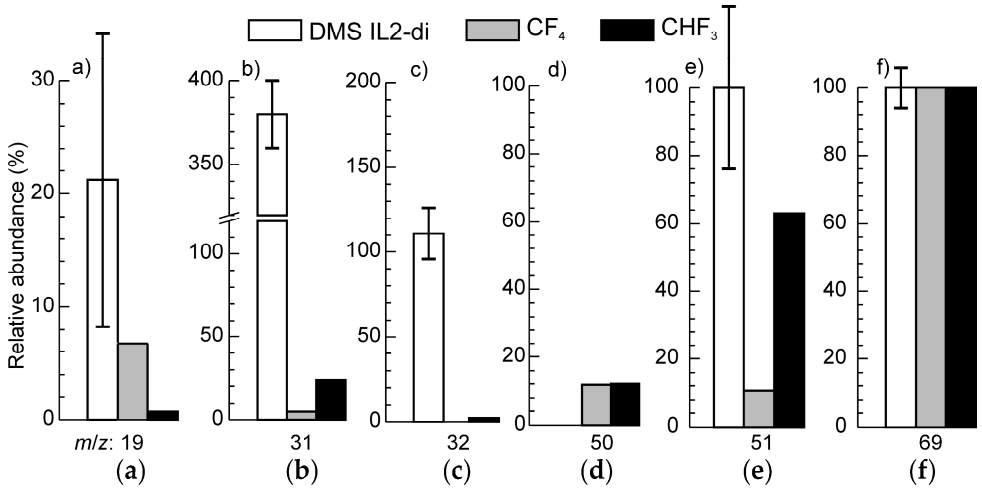

Figure 4. Relative intensities of signals from the group A and fragmentation patterns for electron impact ionization for CF_4 and CHF_3, adapted from [59]. The figures (**a**), (**b**), (**c**), (**d**), (**e**) and (**f**) correspond to the ions with m/z 19, 31, 32, 50, 51 and 69, respectively. All the data were normalized by the signal m/z 69.

Good correlation was also found between the relative intensities of the signals of group B and the fragmentation pattern for methane (Figure 5). The correct proportion between the ions at m/z 15 and 16 indicates that these ions come from methane rather than from higher alkanes, for which the signal at m/z 16 is lacking. Methane can be formed from methyl radicals in a two-step reaction: (i) detachment from the butyl side chains of the cations; and (ii) recombination with hydrogen atoms extracted from the environment, e.g., from the acidic C(2) position on the imidazolium ring [60,61]. This process is promoted by the poor proton abstracting ability of the NTf_2 anion [62]. Previously this model was put forward to explain tribochemical emissions of methane from *N*-alkylimidazolium bis(trifluoromethanesulfonyl)imide ILs and IL2 [27,44,48]. The ethyl group of PEG could be another precursor of methane. The methyl radicals detached from PEG have to undergo complete recombination before they reach the mass spectrometer as it is evidenced from the ratio between m/z 15 and 16 being very close to the reference for methane.

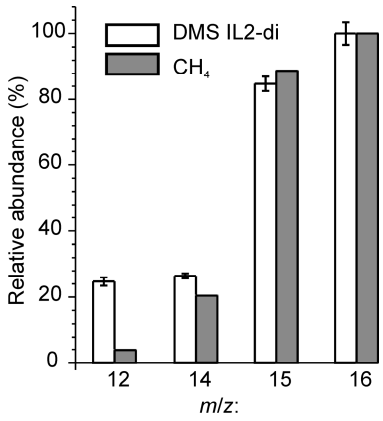

Figure 5. Relative intensities of signals from group B and fragmentation patterns for electron impact ionization for CH_4 adapted from [59]. All the data were normalized by the signal m/z 16.

The excess of ions at m/z 12 and 14 can be related with the presence of butyl (C4) and propyl (C3) radicals among the emitted gas species. These radicals can originate from homolytic cleavage of C–C or C–N bonds at the butyl side chain attached to the cation. Previously it was suggested that part of C3 and C4 can reach a mass spectrometer in a radical form due to their lower reactivity in comparison with methyl [44]. The radical stabilization increases with the increasing number of alkyl substituents on a radical centre because of hyperconjucation [63]. Due to the specifics of detachment from butyl side chains, C3 and C4 radicals should have one methyl and two or three methylene groups. Thus, the mass spectrum of C3 and C4 radicals should have an excess of the ions at m/z 12–14 at the cost of the ions at m/z 15.

Correct attribution of the components of the group C to the ion fragments is not an easy task due to the large number of possible precursors, which can be emitted from the IL in molecular, radical or ionic forms. In the case of IL2 [44], the peaks m/z 24–48 were ascribed to a mixture of C2–C3 alkanes, their radicals and the products of non-oxidative decomposition of PEG, including methyl and ethyl alcohols, noncyclic ethers, formaldehyde, acetic aldehyde, ethylene oxide, and carbon mono- and dioxide, among others [64]. The relative intensities of the components with m/z 24–34 determined in this study matched well the DMS of IL2 [44], but the DMS of IL2-di and IL2 differed in the range m/z 37–48. For IL2 the highest peak was at m/z 43, whereas for IL2-di it was at m/z 44. In comparison with IL2 the relative intensity of m/z 44 rose almost five-fold. This component can be ascribed to the ions $C_3H_8^+$, $C_2H_4O^+$ and CO_2^+. The ion $C_3H_8^+$ is the principal ionized fragment of butane under electron ionization [59] and can originate from the butyl side chain of the cation. For each cation IL2-di has twice the butyl groups as IL2. In the literature, there is no information on the fragmentation patterns of alkyl and ethoxy radicals. However, it is reasonable to suggest that if butyl arrives at a mass spectrometer as radical, the main ionized fragment could be the same as for butane, i.e., $C_3H_8^+$. This is because the dissociation enthalpies of bonds adjacent to a radical centre decrease on 50–70 kcal/mole [63] and the dissociation under electron impact should be localized at the C–C· bond. A PEG monomer–$(CH_2)(CH_2)$O–can be detached from the polymer chain via tribochemical bond scission. This processes relies on the bond stretching that reduces the thermal energy required for cleavage of a bond [65,66]. In PEG, bond cleavage occurs mainly at C–O. This is evident from the fact that CH_4O^+ and $C_2H_4O^+$ with m/z 32 and 44, respectively, were the principal mass-spectral components for volatile products of nonoxidative pyrolysis of PEG [67]. If the detached monomer is further non-dissociatively ionized at the mass-spectrometer the ion $C_2H_4O^+$ with m/z 44 can be formed. This differs from the electron ionization of PEG, which yields $C_2H_5O^+$ with m/z 45 as the principal component. Finally, a significant contribution from carbon dioxide is not expected since oxidative processes are hindered in the vacuum. The difference between IL2 and IL2-di imply that the tribochemical stability of the PEG chain decreased in dicationic configuration. This finding is in line

with the results on the thermal stability of dicationic ILs. Mahrova et al. [46] reported that the thermal stability of dicationic *N*-alkylpyridinium ILs with PEG bridging chains decreased in comparison with an equivalent monocationic *N*-alkylpyridinium IL. Patil and coworkers [31] studied imidazolium, pyrrolidinium and phosphonium dicationic ILs with various lengths of alkane linkage chains and found that the maximum thermal stability corresponded to C9 and decreased with a further increase of the linkage chain length.

The emission of imidazolium head groups or its components could not be detected in this work in the range of m/z 1–120, which accords with previous studies on tribochemical degradation [44,53], but contrasts with thermal [62] and X-ray radiation induced chemical degradation of *N*-alkylimidazolium cations [68]. The slightly lower chemical stability of IL2-di can favour the passivation of metal surfaces and improve wear resistance.

For both IL2-di and IL2 the patterns of the NTf_2 anion tribochemical decomposition were similar. This can be related with the fact that the structure of the anion seems to be insensitive to the length of the linkage chain as well as to the number of the imidazolium head groups in the cation [30]. The results of the present study support the conclusions drawn in the previous work [44], that the detachment of trifluoromethyl was the principal mechanism of the NTf_2 anion degradation on Ti substrates, and contrasted with the findings of the work [27], in which NTf_2 tribochemical degradation on zirconia substrate was accompanied by emission of sulphates and/or sulphite. The difference in the degradation steps of the anion on different substrates could be linked to the bond strength between the anion and the substrate. The anion can be immobilized on a hydroxyl-terminated oxide surface by strong covalent bonding [27,33,69,70], while on a partly oxidized metal surface only physical or chemical adsorption and hydrogen bonding occur. A covalently bonded anion can be subjected to larger strain under interfacial shearing and undergo more significant degradation than an adsorbed anion. It is worth mentioning the similarity of the volatile products for the tribochemical degradation of the anion observed in the present work and X-ray radiation induced chemical degradation reported by Keppler et al. [68]. Both of these processes significantly differ from thermal degradation, which initiates from SO_2 release [62].

Deeper insight into the origin of various ions in the DMS as well as the tribochemical processes lying behind them can be gained using behavioral analysis of the time series of the DMS signals [44]. Figure 6 shows several typical behaviors measured at two normal loads. In contrast with the IL2, the signals did not show well-defined behavioral patterns, rather complex behaviors, which can be characterized by the superposition of various elemental patterns. At the lower load, two behavioral patterns were identified (Figure 6b,c). The first one showed an intensive burst just at the beginning of rubbing followed by a transitional decay, which ceased even before the rubbing end. The mass-spectral components with m/z 15, 51 and 69 (CH_3^+, CHF_2^+, CF_3^+), among others, behaved according to this pattern. The second pattern was characterized by a step-wise increase at the beginning of rubbing and an almost linear decreasing trend during rubbing. After the rubbing end the signal returned to zero almost instantaneously. The mass-spectral peaks of group C mainly behaved following the second pattern. At the higher loads both patterns drastically changed. In the first pattern (Figure 6c) the signals stabilized after the initial burst. After the rubbing end the signals transitionally returned to zero with characteristic time constants in the range 150–250 s. In the second pattern (Figure 6d) the decreasing trend switched to the growing one. After the rubbing end the signals slowly returned to zero with larger time constants, than in the first pattern.

In addition, a third pattern was identified for the mass-spectral peaks, which did not appear at the lower load and corresponded to hydrogen and water (Figure 6a). This pattern was characterized by a very slow dynamics and certain delays at the beginning of rubbing and at its end. This indicates that water and hydrogen emission was not directly related to tribochemical activation, rather with some secondary reactions. Our previous experiments have shown that the substrate and the pin could not be the sources of hydrogen or water. Neither could it be the IL2-di, since it was kept under vacuum for at least 48 h before the experiment and water emission was not observed under the lower load.

Emission of H_2 and H_2O could be conceivably ascribed to the reactions of fluorohydrogen acid (HF) with Ti and TiO_2 [71]:

$$2Ti + 6HF = 2TiF_3 + 3H_2, \quad (3)$$

$$TiO_2 + 2HF = TiOF_2 + H_2O, \quad (4)$$

whereas HF can be formed as a product of the reaction of the anion with the hydroxyl-terminated surface of the alumina pin [70]. In fact, micro-Raman confocal and X-ray Photoelectron Spectrometry (XPS) analyses revealed the presence of TiF_3 and $TiOF_2$ on worn titanium surfaces lubricated with IL2 and other ILs with fluorinated anions [9,26,44].

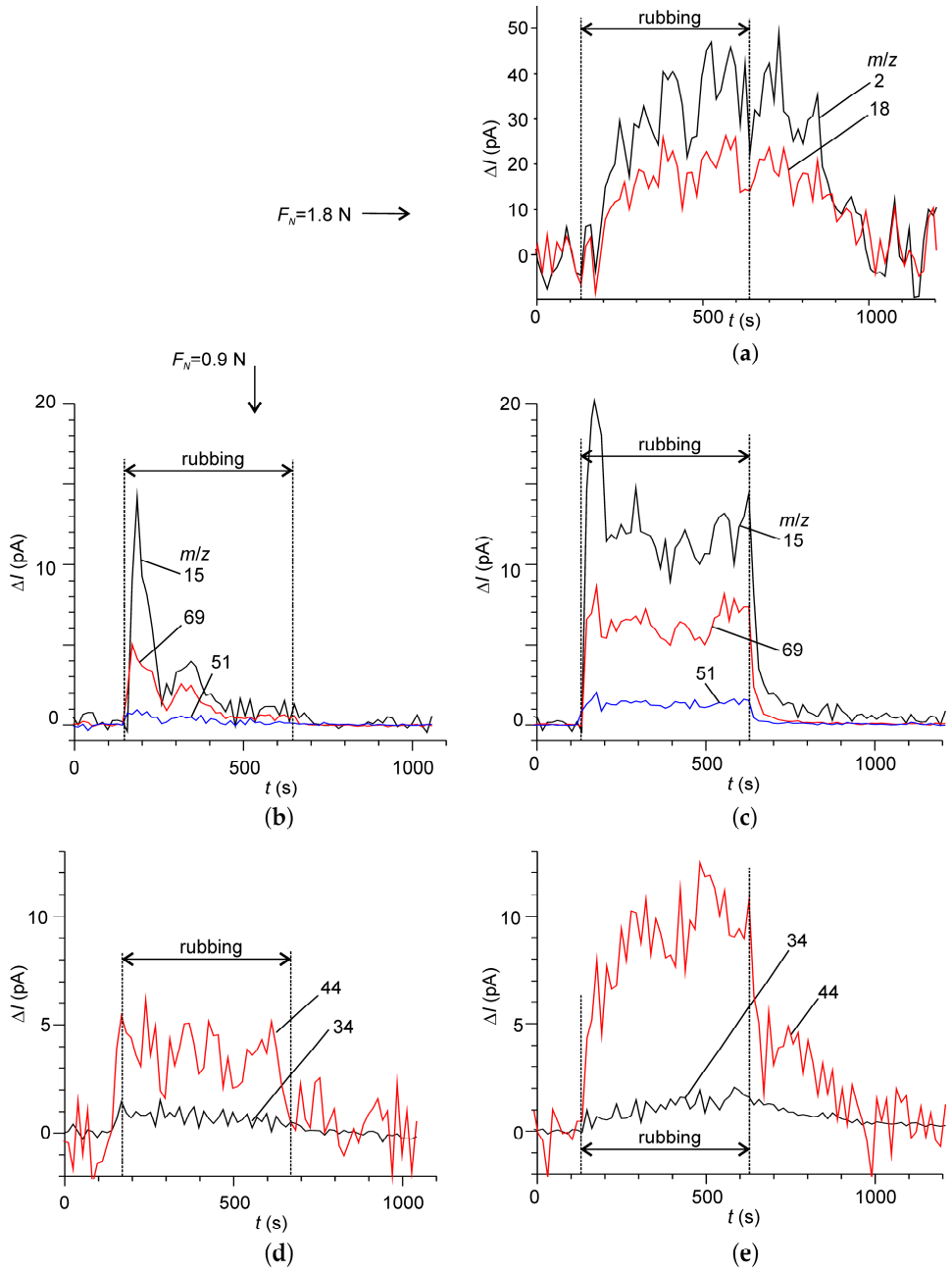

Figure 6. Some typical behavior patterns of the differential mass-spectrometric time series. (**b**,**d**) correspond to the load 0.9 N, whereas (**a**,**c**,**e**) correspond to 1.8 N. The numbers at plot indicate the mass-to-charge ratio, m/z.

Figure 7 shows the upper half of the correlation matrix of the DMS. The values of the Pearson correlation coefficients are codified by four grey levels. White cells correspond to those pairs of signals for which the null hypothesis of the statistical significance of the correlation coefficient was not rejected. Strong correlation can be observed for m/z 2, 17 and 18, which supports the hypothesis of the common precursors and mechanisms of the H_2 and H_2O emissions. Also there is a strong correlation within the following groups: (25, 26, 27), (27, 28, 29) and (30, 31). Moderate correlation can be observed between the peaks of the three groups 14–16, 24–31 and 39–44, as well as between these peaks and m/z 51, 54 and 69. These findings suggest that the processes of anion and cation decomposition for IL2-di are much more strongly correlated than for the monocationic IL2, for which the cationic and anionic decomposition products showed different emission behaviors.

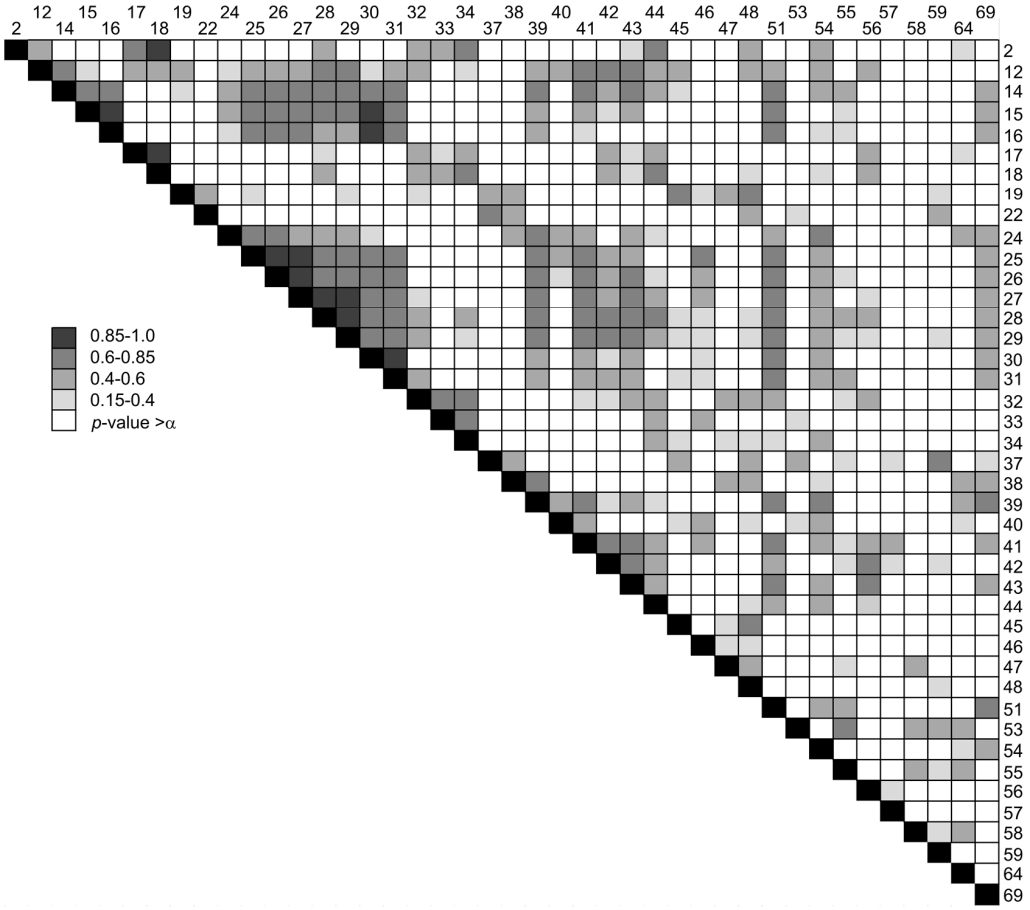

Figure 7. The upper half of the Pearson correlation matrix for the DMS signals. The mass numbers of signals are shown at the rows and columns. The color scale indicates the values of the Pearson coefficient of correlation.

The observed changes in triboemission behavior with the normal load could be interpreted in terms of the formation and wearing off the protective tribofilm. Under the given mild experimental conditions, frictional heating should be discarded as a driving force of tribochemical reactions [72–74]. It should be noted that under low sliding velocity, like in this study, the molecules in the liquid phase could not be strained sufficiently high to trigger tribochemical reactions. Only the molecules bonded to the surface could be subjected to the strain high enough for initiation of tribochemical processes. Thus, the volatiles detected in this study had to originate from the tribofilm. Although a tribofilm was not analysed in this study, there is plenty of experimental evidence that dicationic ILs with longer bridging chains tend to adsorb on the surface, creating large aggregate structures and exhibiting better

packing than monocationic ILs [29,75]. The better lubricity of the IL2-di in comparison with the IL2 can be associated with these compact aggregate structures and the higher surface activity of dicationic ILs with larger spacer lengths [75]. Under the lower normal load, compact aggregate structures could probably accommodate the interfacial shear and protect the substrate from damage. Weak bonding between the ions in the aggregate layer prevented the anions from stretching and from intensive tribochemical decomposition. Thus, after a short run in, the emission of the decomposition products corresponding to the anion completely ceased. On the other hand, the emission of fragments of the side and the bridging chains of the cationic moiety could be related to distinguishing features of the molecular structure of the dicationic ILs. For longer bridging chains, e.g., larger than six methylene groups, two imidazolium rings tended to position themselves above and below each over forming π–π stacking interactions, and the bridge chain extended perpendicularly to the imidazolium ring [38]. In this work we carried out simple molecular mechanics modelling using Chem3D Pro in order to determine the optimal 3-dimensional arrangement of atoms in the isolated cation representing a local energy minimum. The results are shown in Figure 8. Although only a single cation was modelled and the electrons were not explicitly considered in the modelling, in the majority of stable molecular conformations found by the modelling, the cation tended to fold over the PEG bridging chain with two imidazolium heads approaching each other.

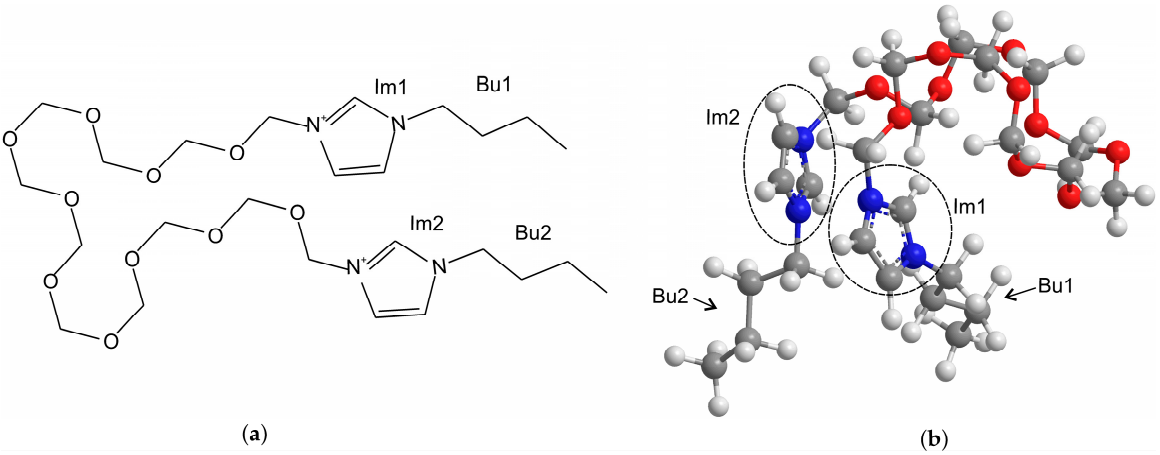

Figure 8. Optimized 3-dimensional stable molecular conformation of the cation of dicationic IL representing a local energy minimum. (**a**) 2-dimensional structure; (**b**) 3-dimensional structure. Im1 and Im2 are the imidazolium head groups; Bu1 and Bu2 are the butyl side chains. The atoms are represented by the following colors: H—white, C—grey, N—blue and O—red.

Some chain–chain interaction was reported for alkyl chains with 12 or more methylene groups [30]. The conformation of the cation with the imidazolium heads bonded to each other and to a substrate, and the side and the bridging chains protruding outside, can probably be a reason for the continuous emission of cationic fragments even under low load. With the increasing normal load, both the cation and anion degradation intensified. On the other hand, removal of the aggregate adsorbed layer under a higher load could allow HF to attack the surface. Slow dynamics of water and hydrogen emission could be related with slow diffusion through the IL followed by desorption from its surface.

4. Conclusions

Mechanically stimulated gas emission spectrometry was applied for the study of dynamic triboemission processes in geminal dicationic IL with *N*-alkylimidazolioum cation head groups, PEG bridging chains and bis(trifluoromethanesulfonyl)imide anions. Homologous monocationic IL was taken as a benchmark. It was found that dicationic IL had better lubricity. The friction coefficient was stable without noticeable run in. The general structures of the mass spectra of volatile components

emitted from the dicationic and monocationic ILs were alike. However, the dicationic IL had a much stronger peak at m/z 44, which was ascribed to a monomer of PEG and butyl. This implies less tribochemical stability of PEG as a bridging chain, than a side chain. The tribochemical decomposition of the anion seemed insensitive to the number of cationic head groups. The behavior of the mass-spectral time series significantly varied with the applied normal load. At the lower load, the signals tended to decrease during rubbing, while at the higher load they increased. In contrast with the homologous monocationic IL, the time series of the ions originating from the cation and anion precursors showed good correlation. The complex behavior of the mechanically stimulated gas emission was interpreted in terms of the dynamic formation and destruction of a protective tribofilm. Mechanically stimulated gas emission mass spectrometry has been proven to be a powerful tool for the dynamic analysis of complex tribochemical processes.

Acknowledgments: The authors are grateful to M. Mahrova for providing the synthesized IL. The authors acknowledge the help of O. Sanchez in measuring the surface profiles. This work was supported by the Ministry of Economy and Competitiveness of Spain through the grant BIA2016-79528-R.

Author Contributions: Roman Nevshupa and Marcello Conte conceived, designed and performed the experiments; Silvia Guerra participated in performing the experiments and data treatment; Roman Nevshupa and Silvia Guerra analyzed the data; Elisa Roman contributed to the analysis and interpretation of the data; Roman Nevshupa wrote the paper.

Conflicts of Interest: The authors declare no conflict of interest.

References

1. Arias-Pardilla, J.; Espinosa, T.; Bermúdez, M.D. Applications: Ionic liquids in surface protection. In *Electrochemistry in Ionic Liquids: Volume 2: Applications*; Springer: Berlin, Germany, 2015; pp. 530–561.
2. Somers, A.; Howlett, P.; MacFarlane, D.; Forsyth, M. A review of ionic liquid lubricants. *Lubricants* **2013**, *1*, 3–21. [CrossRef]
3. Mordukhovich, G.; Qu, J.; Howe, J.Y.; Bair, S.; Yu, B.; Luo, H.; Smolenski, D.J.; Blau, P.J.; Bunting, B.G.; Dai, S. A low-viscosity ionic liquid demonstrating superior lubricating performance from mixed to boundary lubrication. *Wear* **2013**, *301*, 740–746. [CrossRef]
4. Gutierrez, M.; Haselkorn, M.; Iglesias, P. The lubrication ability of ionic liquids as additives for wind turbine gearboxes oils. *Lubricants* **2016**, *4*, 14. [CrossRef]
5. Yu, B.; Bansal, D.G.; Qu, J.; Sun, X.; Luo, H.; Dai, S.; Blau, P.J.; Bunting, B.G.; Mordukhovich, G.; Smolenski, D.J. Oil-miscible and non-corrosive phosphonium-based ionic liquids as candidate lubricant additives. *Wear* **2012**, *289*, 58–64. [CrossRef]
6. Somers, A.; Yunis, R.; Armand, M.; Pringle, J.; MacFarlane, D.; Forsyth, M. Towards phosphorus free ionic liquid anti-wear lubricant additives. *Lubricants* **2016**, *4*, 22. [CrossRef]
7. Huang, G.; Yu, Q.; Ma, Z.; Cai, M.; Liu, W. Probing the lubricating mechanism of oil-soluble ionic liquids additives. *Tribol. Int.* **2017**, *107*, 152–162. [CrossRef]
8. Cai, M.; Liang, Y.; Yao, M.; Xia, Y.; Zhou, F.; Liu, W. Imidazolium ionic liquids as antiwear and antioxidant additive in poly(ethylene glycol) for steel/steel contacts. *ACS Appl. Mater. Interfaces* **2010**, *2*, 870–876. [CrossRef] [PubMed]
9. Gabler, C.; Dörr, N.; Allmaier, G. Influence of cationic moieties on the tribolayer constitution shown for bis(trifluoromethylsulfonyl)imide based ionic liquids studied by X-ray photoelectron spectroscopy. *Tribol. Int.* **2014**, *80*, 90–97. [CrossRef]
10. Pisarova, L.; Gabler, C.; Dörr, N.; Pittenauer, E.; Allmaier, G. Thermo-oxidative stability and corrosion properties of ammonium based ionic liquids. *Tribol. Int.* **2012**, *46*, 73–83. [CrossRef]
11. Minami, I. Ionic liquids in tribology. *Molecules* **2009**, *14*, 2286–2305. [CrossRef] [PubMed]
12. Morales, W.; Street, K.W.J.; Rychard, R.M.; Valco, D. Tribological testing and thermal analysis of an alkyl sulfate series of ionic liquids for use as aerospace lubricants. *Tribol. Trans.* **2012**, *55*, 815–821. [CrossRef]
13. Zhang, S.; Hu, L.; Qiao, D.; Feng, D.; Wang, H. Vacuum tribological performance of phosphonium-based ionic liquids as lubricants and lubricant additives of multialkylated cyclopentanes. *Tribol. Int.* **2013**, *66*, 289–295. [CrossRef]

14. Jin, C.-M.; Ye, C.; Phillips, B.S.; Zabinski, J.S.; Liu, X.; Liu, W.; Shreeve, J.N.M. Polyethylene glycol functionalized dicationic ionic liquids with alkyl or polyfluoroalkyl substituents as high temperature lubricants. *J. Mater. Chem.* **2006**, *16*, 1529–1535. [CrossRef]
15. Jiménez, A.; Bermúdez, M.-D. Ionic liquids as lubricants of titanium—Steel contact. *Tribol. Lett.* **2009**, *33*, 111–126. [CrossRef]
16. Jiménez, A.E.; Bermúdez, M.D.; Iglesias, P.; Carrión, F.J.; Martínez-Nicolás, G. 1-N-alkyl-3-methylimidazolium ionic liquids as neat lubricants and lubricant additives in steel—Aluminium contacts. *Wear* **2006**, *260*, 766–782. [CrossRef]
17. Jiménez, A.-E.; Bermúdez, M.-D. Imidazolium ionic liquids as additives of the synthetic ester propylene glycol dioleate in aluminium—Steel lubrication. *Wear* **2008**, *265*, 787–798. [CrossRef]
18. Barnhill, W.C.; Qu, J.; Luo, H.; Meyer, H.M.; Ma, C.; Chi, M.; Papke, B.L. Phosphonium-organophosphate ionic liquids as lubricant additives: Effects of cation structure on physicochemical and tribological characteristics. *ACS Appl. Mater. Interfaces* **2014**, *6*, 22585–22593. [CrossRef] [PubMed]
19. Pejaković, V.; Tomastik, C.; Dörr, N.; Kalin, M. Influence of concentration and anion alkyl chain length on tribological properties of imidazolium sulfate ionic liquids as additives to glycerol in steel–steel contact lubrication. *Tribol. Int.* **2016**, *97*, 234–243. [CrossRef]
20. Mu, Z.; Zhou, F.; Zhang, S.; Liang, Y.; Liu, W. Effect of the functional groups in ionic liquid molecules on the friction and wear behavior of aluminum alloy in lubricated aluminum-on-steel contact. *Tribol. Int.* **2005**, *38*, 725–731. [CrossRef]
21. Cai, M.; Zhao, Z.; Liang, Y.; Zhou, F.; Liu, W. Alkyl imidazolium ionic liquids as friction reduction and anti-wear additive in polyurea grease for steel/steel contacts. *Tribol. Lett.* **2010**, *40*, 215–224. [CrossRef]
22. Xiao, H.; Guo, D.; Liu, S.; Pan, G.; Lu, X. Film thickness of ionic liquids under high contact pressures as a function of alkyl chain length. *Tribol. Lett.* **2011**, *41*, 471–477. [CrossRef]
23. Fan, M.; Song, Z.; Liang, Y.; Zhou, F.; Liu, W. Laxative inspired ionic liquid lubricants with good detergency and no corrosion. *ACS Appl. Mater. Interfaces* **2014**, *6*, 3233–3241. [CrossRef] [PubMed]
24. Ye, C.; Liu, W.; Chen, Y.; Yu, L. Room-temperature ionic liquids: A novel versatile lubricant. *Chem. Commun.* **2001**, 2244–2245. [CrossRef]
25. Zhou, F.; Liang, Y.; Liu, W. Ionic liquid lubricants: Designed chemistry for engineering applications. *Chem. Soc. Rev.* **2009**, *38*, 2590–2599. [CrossRef] [PubMed]
26. Jiménez, A.E.; Bermúdez, M.D. Ionic liquids as lubricants of titanium—Steel contact. Part 3. Ti6Al4V lubricated with imidazolium ionic liquids with different alkyl chain lengths. *Tribol. Lett.* **2010**, *40*, 237–246. [CrossRef]
27. Mahrova, M.; Conte, M.; Roman, E.; Nevshupa, R. Critical insight into mechanochemical and thermal degradation of imidazolium-based ionic liquids with alkyl and monomethoxypoly(ethylene glycol) side chains. *J. Phys. Chem. C* **2014**, *118*, 22544–22552. [CrossRef]
28. Li, S.; Feng, G.; Bañuelos, J.L.; Rother, G.; Fulvio, P.F.; Dai, S.; Cummings, P.T. Distinctive nanoscale organization of dicationic versus monocationic ionic liquids. *J. Phys. Chem. C* **2013**, *117*, 18251–18257. [CrossRef]
29. Shirota, H.; Ishida, T. Microscopic aspects in dicationic ionic liquids through the low-frequency spectra by femtosecond Raman-induced KERR effect spectroscopy. *J. Phys. Chem. B* **2011**, *115*, 10860–10870. [CrossRef] [PubMed]
30. Bodo, E.; Chiricotto, M.; Caminiti, R. Structure of geminal imidazolium bis(trifluoromethylsulfonyl)imide dicationic ionic liquids: A theoretical study of the liquid phase. *J. Phys. Chem. B* **2011**, *115*, 14341–14347. [CrossRef] [PubMed]
31. Patil, R.A.; Talebi, M.; Xu, C.; Bhawal, S.S.; Armstrong, D.W. Synthesis of thermally stable geminal dicationic ionic liquids and related ionic compounds: An examination of physicochemical properties by structural modification. *Chem. Mater.* **2016**, *28*, 4315–4323. [CrossRef]
32. Pagano, F.; Gabler, C.; Zare, P.; Mahrova, M.; Dörr, N.; Bayon, R.; Fernandez, X.; Binder, W.; Hernaiz, M.; Tojo, E.; et al. Dicationic ionic liquids as lubricants. *J. Eng. Tribol.* **2012**, *226*, 952–964. [CrossRef]
33. Palacio, M.; Bhushan, B. Molecularly thick dicationic ionic liquid films for nanolubrication. *J. Vac. Sci. Technol. A* **2009**, *27*, 986–995. [CrossRef]
34. Czerniak, K.; Walkiewicz, F. Synthesis and antioxidant properties of dicationic ionic liquids. *New J. Chem.* **2017**, *41*, 530–539. [CrossRef]

35. Chang, J.-C.; Ho, W.-Y.; Sun, I.W.; Tung, Y.-L.; Tsui, M.-C.; Wu, T.-Y.; Liang, S.-S. Synthesis and characterization of dicationic ionic liquids that contain both hydrophilic and hydrophobic anions. *Tetrahedron* **2010**, *66*, 6150–6155. [CrossRef]
36. Gindri, I.M.; Siddiqui, D.A.; Frizzo, C.P.; Martins, M.A.P.; Rodrigues, D.C. Improvement of tribological and anti-corrosive performance of titanium surfaces coated with dicationic imidazolium-based ionic liquids. *RSC Adv.* **2016**, *6*, 78795–78802. [CrossRef]
37. Khan, A.S.; Man, Z.; Arvina, A.; Bustam, M.A.; Nasrullah, A.; Ullah, Z.; Sarwono, A.; Muhammad, N. Dicationic imidazolium based ionic liquids: Synthesis and properties. *J. Mol. Liq.* **2017**, *227*, 98–105. [CrossRef]
38. Serva, A.; Migliorati, V.; Lapi, A.; Aquilanti, G.; Arcovito, A.; D'Angelo, P. Structural properties of geminal dicationic ionic liquid/water mixtures: A theoretical and experimental insight. *Phys. Chem. Chem. Phys.* **2016**, *18*, 16544–16554. [CrossRef] [PubMed]
39. Anderson, J.L.; Ding, R.; Ellern, A.; Armstrong, D.W. Structure and properties of high stability geminal dicationic ionic liquids. *J. Am. Chem. Soc.* **2005**, *127*, 593–604. [CrossRef] [PubMed]
40. Shirota, H.; Mandai, T.; Fukazawa, H.; Kato, T. Comparison between dicationic and monocationic ionic liquids: Liquid density, thermal properties, surface tension, and shear viscosity. *J. Chem. Eng. Data* **2011**, *56*, 2453–2459. [CrossRef]
41. Zeng, Z.; Phillips, B.S.; Xiao, J.-C.; Shreeve, J.N.M. Polyfluoroalkyl, polyethylene glycol, 1,4-bismethylenebenzene, or 1,4-bismethylene-2,3,5,6-tetrafluorobenzene bridged functionalized dicationic ionic liquids: Synthesis and properties as high temperature lubricants. *Chem. Mater.* **2008**, *20*, 2719–2726. [CrossRef]
42. Minami, I.; Inada, T.; Sasaki, R.; Nanao, H. Tribo-chemistry of phosphonium-derived ionic liquids. *Tribol. Lett.* **2010**, *40*, 225–235. [CrossRef]
43. Jiménez, A.E.; Bermúdez, M.D. Short alkyl chain imidazolium ionic liquid additives in lubrication of three aluminium alloys with synthetic ester oil. *Tribol. Mater. Surf. Interfaces* **2012**, *6*, 109–115. [CrossRef]
44. Nevshupa, R.; Conte, M.; del Campo, A.; Roman, E. Analysis of tribochemical decomposition of two imidazolium ionic liquids on Ti–6Al–4V through mechanically stimulated gas emission spectrometry. *Tribol. Int.* **2016**, *102*, 19–27. [CrossRef]
45. Cai, M.; Liang, Y.; Zhou, F.; Liu, W. A novel imidazolium salt with antioxidation and anticorrosion dual functionalities as the additive in poly(ethylene glycol) for steel/steel contacts. *Wear* **2013**, *306*, 197–208. [CrossRef]
46. Mahrova, M.; Pagano, F.; Pejakovic, V.; Valea, A.; Kalin, M.; Igartua, A.; Tojo, E. Pyridinium based dicationic ionic liquids as base lubricants or lubricant additives. *Tribol. Int.* **2015**, *82*, 245–254. [CrossRef]
47. Bermúdez, M.-D.; Jiménez, A.-E.; Sanes, J.; Carrión, F.-J. Ionic liquids as advanced lubricant fluids. *Molecules* **2009**, *14*, 2888–2908. [CrossRef] [PubMed]
48. Lu, R.; Mori, S.; Kobayashi, K.; Nanao, H. Study of tribochemical decomposition of ionic liquids on a nascent steel surface. *Appl. Surf. Sci.* **2009**, *255*, 8965–8971. [CrossRef]
49. Nevchoupa, R.A.; De Segovia, J.L.; Deulin, E.A. An UHV system to study gassing and outgassing of metals under friction. *Vacuum* **1999**, *52*, 73–81. [CrossRef]
50. Nevshupa, R.A.; Conte, M.; Igartua, A.; Roman, E.; de Segovia, J.L. Ultrahigh vacuum system for advanced tribology studies: Design principles and applications. *Tribol. Int.* **2015**, *86*, 28–35. [CrossRef]
51. Okubo, H.; Sasaki, S. In situ raman observation of structural transformation of diamond-like carbon films lubricated with modtc solution: Mechanism of wear acceleration of DLC films lubricated with MoDTC solution. *Tribol. Int.* **2017**, *113*, 399–410. [CrossRef]
52. Merkle, A.P.; Erdemir, A.; Eryilmaz, O.L.; Johnson, J.A.; Marks, L.D. In situ TEM studies of tribo-induced bonding modifications in near-frictionless carbon films. *Carbon* **2010**, *48*, 587–591. [CrossRef]
53. Kawada, S.; Watanabe, S.; Kondo, Y.; Tsuboi, R.; Sasaki, S. Tribochemical reactions of ionic liquids under vacuum conditions. *Tribol. Lett.* **2014**, *54*, 309–315. [CrossRef]
54. Nevshupa, R.; Grinkevich, K.E.; Martinez, I.; Roman, E. Trides—A new tool for the design, development and non-destructive evaluation of advanced construction steels. *Mater. Constr.* **2016**, *66*, e099. [CrossRef]
55. Zare, P.; Mahrova, M.; Tojo, E.; Stojanovic, A.; Binder, W.H. Ethylene glycol-based ionic liquids via azide/alkyne click chemistry. *J. Polym. Sci. Part A Polym. Chem.* **2013**, *51*, 190–202. [CrossRef]

56. Nevshupa, R.A.; Roman, E.; de Segovia, J.L. Origin of hydrogen desorption during friction of stainless steel by alumina in ultrahigh vacuum. *J. Vac. Sci. Technol. A* **2008**, *26*, 1218–1223. [CrossRef]
57. Rusanov, A.; Nevshupa, R.; Fontaine, J.; Martin, J.-M.; Le Mogne, T.; Elinson, V.; Lyamin, A.; Roman, E. Probing the tribochemical degradation of hydrogenated amorphous carbon using mechanically stimulated gas emission spectroscopy. *Carbon* **2015**, *81*, 788–799. [CrossRef]
58. Roman, E.; Conte, M.; Nevshupa, R. *Proceedings of Lubmat: Lubrication, Maintenance and Tribology, Bilbao, Spain, 7–8 June 2016*; Aranzabe, A., Ed.; IK4-Tekniker: Bilbao, Spain, 2016; p. 620.
59. Stein, S.E. "Mass spectra" by nist mass spec data center. In *NIST Chemistry Webbook NIST, Standard Reference Database Number 69*; Linstrom, P.J., Mallard, W.G., Eds.; National Institute of Standards and Technology: Gaithersburg, MD, USA, 2017.
60. Rusanov, A.; Nevshupa, R.; Martin, J.-M.; Garrido, M.Á.; Roman, E. Tribochemistry of hydrogenated amorphous carbon through analysis of mechanically stimulated gas eission. *Diam. Relat. Mater.* **2015**, *55*, 32–40. [CrossRef]
61. Köddermann, T.; Wertz, C.; Heintz, A.; Ludwig, R. Ion-pair formation in the ionic liquid 1-ethyl-3-methylimidazolium bis(triflyl)imide as a function of temperature and concentration. *ChemPhysChem* **2006**, *7*, 1944–1949. [CrossRef] [PubMed]
62. Kroon, M.C.; Buijs, W.; Peters, C.J.; Witkamp, G.-J. Quantum chemical aided prediction of the thermal decomposition mechanisms and temperatures of ionic liquids. *Thermochim. Acta* **2007**, *465*, 40–47. [CrossRef]
63. Zhang, X.-M. Homolytic bond dissociation enthalpies of the c-h bonds adjacent to radical centers. *J. Org. Chem.* **1998**, *63*, 1872–1877. [CrossRef]
64. Pielichowski, K.; Flejtuch, K. Non-oxidative thermal degradation of poly(ethylene oxide): Kinetic and thermoanalytical study. *J. Anal. Appl. Pyrolysis* **2005**, *73*, 131–138. [CrossRef]
65. Boldyrev, V.V. Mechanochemistry and mechanical activation of solids. *Russ. Chem. Rev.* **2006**, *75*, 177–190. [CrossRef]
66. Ribas-Arino, J.; Marx, D. Covalent mechanochemistry: Theoretical concepts and computational tools with applications to molecular nanomechanics. *Chem. Rev.* **2012**, *112*, 5412–5487. [CrossRef] [PubMed]
67. Kitahara, Y.; Takahashi, S.; Fujii, T. Thermal analysis of polyethylene glycol: Evolved gas analysis with ion attachment mass spectrometry. *Chemosphere* **2012**, *88*, 663–669. [CrossRef] [PubMed]
68. Keppler, A.; Himmerlich, M.; Ikari, T.; Marschewski, M.; Pachomow, E.; Hofft, O.; Maus-Friedrichs, W.; Endres, F.; Krischok, S. Changes of the near-surface chemical composition of the 1-ethyl-3-methylimidazolium bis(trifluoromethylsulfonyl)imide room temperature ionic liquid under the influence of irradiation. *Phys. Chem. Chem. Phys.* **2011**, *13*, 1174–1181. [CrossRef] [PubMed]
69. Nainaparampil, J.J.; Phillips, B.S.; Eapen, K.C.; Zabinski, J.S. Micro–nano behaviour of dmbi-pf 6 ionic liquid nanocrystals: Large and small-scale interfaces. *Nanotechnology* **2005**, *16*, 2474. [CrossRef]
70. Valkenberg, M.H.; deCastro, C.; Holderich, W.F. Immobilisation of ionic liquids on solid supports. *Green Chem.* **2002**, *4*, 88–93. [CrossRef]
71. Buslaev, Y.A.; Bochkareva, V.A.; Nikolaev, N.S. The reaction of titanium dioxide with hydrofluoric acid. *Russ. Chem. Bull.* **1962**, *11*, 361–364. [CrossRef]
72. Walton, A.J. Triboluminescence. *Adv. Phys.* **1977**, *26*, 887–948. [CrossRef]
73. Nevshupa, R. The role of athermal mechanisms in the activation of tribodesorption and triboluminisence in miniature and lightly loaded friction units. *J. Frict. Wear* **2009**, *30*, 118–126. [CrossRef]
74. Nevshupa, R.A.; Roman, E.; de Segovia, J.L. Model of the effect of local frictional heating on the tribodesorbed gases from metals in ultra-high vacuum. *Int. J. Mater. Prod. Technol.* **2010**, *38*, 57–65. [CrossRef]
75. Frizzo, C.P.; Gindri, I.M.; Bender, C.R.; Tier, A.Z.; Villetti, M.A.; Rodrigues, D.C.; Machado, G.; Martins, M.A.P. Effect on aggregation behavior of long-chain spacers of dicationic imidazolium-based ionic liquids in aqueous solution. *Colloids Surf. A Physicochem. Eng. Asp.* **2015**, *468*, 285–294. [CrossRef]